Materials Today Communications 52 (2026) 115193

Contents lists available at ScienceDirect

Materials Today Communications

journal homepage: www.elsevier.com/locate/mtcomm

From mineralogy to functionality: Sicilian clays as structurally-driven suspensions for topical delivery of resveratrol

Claudio Finocchiaro [a], Debora Santonocito [b], Salvatore Barreca [c], Giuseppe Maccarrone [c], Lucia Montenegro [b], Carmelo Puglia [b], Rosario Pignatello [b], Antonino Chindemi [a], Paolo Mazzoleni [a,*], Germana Barone [a]

[a] Department of Biological, Geological and Environmental Sciences, University of Catania, Italy
[b] Department of Drug and Health Sciences, University of Catania, Italy
[c] Department of Chemical Sciences, University of Catania, Italy

ARTICLE INFO

Keywords:
Clay
Mineralogy
Resveratrol
Viscometry
Clay-based suspensions

ABSTRACT

For the first time, four unexplored Sicilian clay deposits were investigated through a multidisciplinary approach as potential raw materials for clay-based topical suspensions in a pre-formulation context, to bridge a key gap between mineralogical characterization and functional screening. Particle-size distribution (PSD), chemical, mineralogical and structural characterization was performed using laser granulometry, XRF, ICP-MS, XRD, FT-IR, TGA on both bulk materials and the $\leq$ 2 μm fractions selected for suspension preparation. Varicoloured clays (CALT1 and CALT2) exhibited higher alumina and iron contents and were enriched in interlayered illite/smectite, with CALT1 also containing chlorite, whereas Plio-pleistocene clay (SIL) and grey clays of the Fm. Terravecchia (CEN) were relatively richer in smectite and kaolinite. The $\leq$ 2 μm fractions preserved the main phyllosilicate structures while minimizing coarse, non-clayey minerals (ranging 32–47 wt% in bulk samples), resulting in improved dispersion and more uniform rheological behaviour. Model clay-based dispersions containing resveratrol (0.6% w/w) were prepared in a hydro-alcoholic medium and used to compare technological performance and release behaviour. Preliminary release studies using Franz diffusion cells over 24 h revealed clay-dependent profiles. CALT1 and CALT2 showed the highest and most sustained resveratrol release (22.28 ± 0.003% and 17.32 ± 0.005%, respectively), while SIL and CEN exhibited lower release (16.34 ± 0.245% and 7.52 ± 0.032%). Overall, the results show that both mineralogical composition and PSD contribute to the rheological and release behaviour of the investigated suspensions. The study provides a mineralogy-based pre-formulation screening framework for selecting natural clay materials for future topical delivery applications.

1. Introduction

Clay minerals are phyllosilicates composed of nanometric layers of tetrahedral and octahedral sheets, whose structural arrangements confer distinctive properties such as plasticity, cation exchange capacity (CEC), high surface area and chemical reactivity [1,2]. These features, along with their widespread availability and low environmental impact, have made clays valuable across a wide range of industrial applications, including: ceramics, construction, environmental remediation, pharmaceuticals and cosmetics [3–8]. In the Mediterranean context, Sicily represents a geologically rich and diversified region, with extensive clay deposits [9]. These include significant accumulations of smectite, illite, kaolinite and mixed-layer clays, often associated with marine-lagoonal and hydrothermal environments [10]. The abundance, mineralogical diversity and strategic location of these deposits make them promising candidates for high-value applications [11,12], especially in health-related sectors, yet they remain underutilized beyond traditional uses.

Sicilian clays have long been employed in the ceramic industry, particularly in the production of plate ware and tiles due to their favourable sintering properties [11,13]. More recently, they have shown potential as precursors in alkali-activated materials and geopolymer binders, offering sustainable alternatives to Portland cement in construction and waste stabilization [14]. Despite this, their exploitation for pharmaceutical and cosmetic purposes is still at an early stage, even though natural clays are increasingly sought after as eco-compatible

* Corresponding author.
E-mail address: paolo.mazzoleni@unict.it (P. Mazzoleni).

https://doi.org/10.1016/j.mtcomm.2026.115193
Received 9 February 2026; Received in revised form 13 April 2026; Accepted 14 April 2026
Available online 15 April 2026

excipients and active ingredients in dermo-cosmetic formulations.

The potential use of clays in pharmaceutical and cosmetic applications is, however, not without challenges [15,16]. The presence of crystalline impurities (e.g., quartz, feldspars), microbial contamination and batch-to-batch variability can pose serious safety concerns for topical or oral use [17]. Moreover, insufficient purification, inadequate particle size control and high levels of trace metals (such as Fe, Ni, or Cr) may limit the use of natural clays unless they undergo proper treatment and rigorous quality assessment [18]. The interactions between clay surfaces and active pharmaceutical ingredients (APIs) also require careful evaluation to avoid undesired adsorption or chemical instability [7,19].

Understanding the mineralogical and microstructural properties of clay minerals is essential for their effective application in pharmaceutical and dermo-cosmetic formulations. X-ray diffraction (XRD), as a primary technique, alongside Fourier-transform infrared spectroscopy (FTIR), scanning electron microscopy (SEM) and thermogravimetric analysis (TGA/DSC), provides comprehensive insights into the crystalline phases and purity of clays. These analytical methods are fundamental for correlating structural features with functional performance parameters such as swelling behaviour, cation exchange capacity (CEC), rheological properties and compatibility with active pharmaceutical or cosmetic ingredients. The mineralogical composition directly affects adsorption capacity, swelling behaviour and the interaction with compounds [20]. Optimizing microstructural parameters of drug carriers such as pore volume, particle morphology and layer arrangement is critical for improving drug loading and achieving controlled release [21]. Clays with an optimal pore volume (~0.100 cm^3/g) have demonstrated enhanced adsorption and sustained release performance, while deviations from this threshold reduce efficacy [22]. This study adopts a multidisciplinary approach to investigate selected natural, underexplored Sicilian clays, integrating mineralogical, particle size distribution, physicochemical and functional analyses. Although clay minerals have been widely investigated as pharmaceutical excipients and several studies have explored resveratrol-based delivery systems, the relationship between detailed mineralogical features of natural clays and their functional performance in topical suspensions remains insufficiently explored. In this context, the novelty of this work lies in bridging classical clay mineralogy with early-stage pre-formulation screening by comparing how differences in phyllosilicate assemblage and fine-fraction particle-size distribution affect the behaviour of clay-based topical suspensions loaded with resveratrol.

Rather than developing a finished cosmetic product, the work focuses on an early-stage pre-formulation screening strategy, in which fine clay fractions ($\leq$ 2 μm) are evaluated as potential functional carriers in simplified model dispersions using resveratrol (RSV) as a reference compound. This approach allows isolation of the intrinsic contribution of mineralogical composition and microstructure to key technological properties, including viscosity, spreadability, occlusion and release behaviour. Chemical and mineralogical features were investigated using complementary techniques (XRF, ICP-MS, XRD, FT-IR and TGA), while functional tests were employed to compare the performance of different clay types. The results provide the basis for selecting promising natural clays for future development of topical delivery systems, supporting the sustainable valorisation of local clay resources.

1.1. Sicilian geological setting

Sicily forms part of the south-verging Apenninic-Maghrebian thrust belt, which includes a foreland domain, represented by the undeformed Hyblean Plateau, and an orogenic domain composed of a stack of nappes emplaced during the Paleogene-Neogene in response to the Africa-Europe collision [23]. Based on paleogeographic reconstructions, Finetti et al. identified several tectono-sedimentary complexes in eastern Sicily [24]. From the most external to the most internal zones, these include: (i) the Ionides (Imerese and Mt. Judica Units); (ii) the Panormide Platform Units; (iii) the Alpine Tethydes (Sicilide Units); and (iv) a European plate domain consisting of Variscan metamorphic basement and residues of Mesozoic cover (Kabilo-Calabride Units). In this work, attention is restricted to three clay-rich successions that extensively crop out across Sicily and are considered representative markers of the island's tectono-sedimentary evolution: the Cretaceous variegated clays, the Tortonian Terravecchia Formation and the Plio-Pleistocene pelites. The oldest and most iconic are the variegated clay, a multicoloured mélange of red, green and grey hemipelagic mudstones that were laid down in deep Alpine-Tethyan basins during Cretaceous (145–66 Mya). During Neogene collision, these strata were dragged into the orogenic wedge. Their ductility allowed them to become regional detachment layers, so they now delineate thrust contacts across hundreds of kilometres. Then, along the northern rim of the Caltanissetta Basin, interbedded deposits of the Terravecchia Formation lie. In the Late Tortonian two brief, high-stand pulses of bioclastic-reef carbonate growth drowned deltaic systems [25]. These layers are invaluable chronostratigraphic markers: they pin the timing of thrust propagation and record eustatic oscillations immediately preceding the Messinian salinity crisis. Finally, the Plio-Pleistocene pelites fill the Licata-Gela foredeep and the south-eastern shelf up to several hundred metres, representing the Quaternary phase of rapid subsidence where high sediment-accumulation rates were associated with periodic stagnation events in a semi-enclosed basin [10]. Generally, the variegated clay, the Terravecchia formation and the Plio-Pleistocene clays provide a continuous, that spans the closure of the Alpine Tethys, the Messinian salinity crisis and the ongoing foreland flexure.

2. Materials and methods

2.1. Materials

The clay deposits were selected based on their geological representativeness within Sicily, their availability and their contrasting mineralogical composition, in order to compare different clay assemblages and their influence on functional behaviour. In particular, four Sicilian deposits were sampled (Fig. 1): two varicoloured clays of the Fm. Caltavuturo of the Imerese Unit (Palermo), selected for their peculiar abundance in clayey grainsize fraction and differentiated by their colour, one green (CALT1) and one red (CALT2); one yellowish of Pliopleistocene from Motta Sant'Anastasia (Catania; labelled with SIL) and the last one greyish of Fm. Terravecchia from Centuripe (Enna; named with CEN), for their abundance on the island and for the variable contents in carbonates. Therefore, the study was designed as a comparative screening of geologically distinct natural clay resources. In general, the sampling was carried out manually, removing the first 40 cm of soils to limit superficial contaminations.

2.2. Methods

2.2.1. Bulk mineralogical and chemical characterization

Bulk mineralogy was initially assessed by X-ray diffraction (XRD). Powdered samples were analysed using a Rigaku MiniFlex diffractometer equipped with a Ni-filtered Cu Kα radiation source operating at 40 kV and 15 mA. Diffractograms were collected in the 2θ range of 5–65°, with a scanning speed of 5°/min and a step size of 0.02°. Qualitative and quantitative analyses were performed using the BGMN/Profex 5.0 software package software [27], supported by the BGMN structural database (http://www.bgmn.de/index.html).

Chemical composition was determined using a Rigaku Supermini 200 wavelength-dispersive X-ray fluorescence (XRF) spectrometer on pressed powder pellets. Calibration of the spectrometer was performed using international geological standards. Major elements, reported as oxides (SiO_2, TiO_2, Al_2O_3, Fe_2O_3, CaO, Na_2O, K_2O, P_2O_5), and selected trace elements (Rb, Y, Zr, Nb) were quantitatively assessed.

Loss on ignition (LOI) was gravimetrically measured by heating the

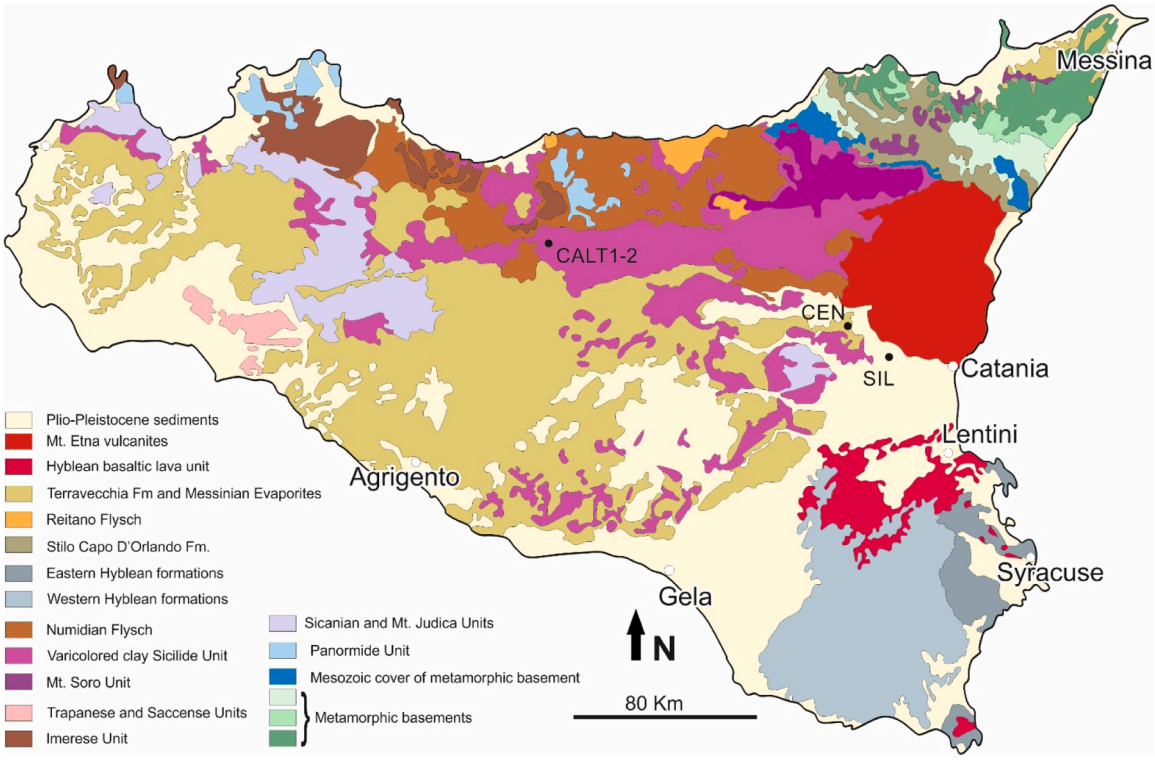

Fig. 1. – Simplified Sicily's geological map (modified from the work of Raneri et al. [26]).

samples overnight at 950 °C.

To ensure no environmental contaminations, trace elements, such as Mg, V, Cr, Mn, Fe, Co, Ni, Cu, Ti, Zn, As, Se, Sr, Cd, Sb, Ba and Pb were determined by means of ICP-MS using an Agilent 8900 instrument after complete acid dissolution of the powders using an HF and HNO_3 mixture.

2.2.2. *Clay separation and mineralogical, spectroscopic and thermal characterization*

Granulometric separation of all samples was carried out to isolate the clay fraction (<2 μm) following Stokes' law. Briefly, powdered material was dispersed in bi-distilled water to prepare an aqueous suspension and the ≤ 2 μm fraction was collected by timed sedimentation. This threshold was selected because it corresponds to the conventional clay-size fraction in mineralogical studies and enables a reproducible comparison of phyllosilicate-rich materials for pre-formulation screening. To further characterise the granulometric properties of the starting deposits, particle-size distribution (PSD) was also measured by a Malvern Mastersizer 3000E laser diffraction particle size analyzer on the < 32 μm fraction, obtained after wet manually sieving. Size descriptors (d10, d50 and d90) were measured to support the interpretation of rheological and functional behaviour.

Afterwards, the desired fractions were subjected to monocationic exchange procedures with a 0.1 M solution of $MgCl_2$ $6H_2O$ for four rinses and with a 50/50 ethanol/water solution to remove excess chloride ions for other two. Oriented clay slides were then prepared using a Millipore™ filtration device following the procedure described by Moore and Reynolds, 1997. Two slides were prepared for each sample, in order to analyse them in air-dry (AD) and ethylene glycol (EG) conditions. This latter allowed to identify the expandable clay minerals through EG intercalation. For this purpose, an oriented slide was exposed to EG vapours at 60 °C for at least 8 h inside a desiccator within an oven. Once AD slides were analysed by XRD, they were thermal treated at 375 °C into a muffle to observe the collapse of clay minerals.

XRD patterns of oriented clays on slides were recorded in the 2θ range from 3° to 35°, using a scanning speed of 2°/min and a step size of 0.01°. Comparison of AD and EG patterns was used to identify and confirm the presence of expandable clay minerals. The degree of interstratification in clay minerals (e.g., illite/smectite, I/S) was categorized according to three ordering levels: R= 0 (disordered), R= 1 (partially ordered), and R= 2 (ordered) [28]. The processing of EG acquisitions, aimed to define the clay minerals and their semi-quantitative amounts, was performed using Newmod software [29].

A 10 mg amount of the monocationic clay samples, previously dried in an oven at 60 °C for 48 h, was mixed with 180 mg of KBr, pre-dried at 110 °C. The mixture was finely ground using an agate mortar until achieving a talc-like powder consistency. The powder was subsequently placed into a sample holder and pressed at a pressure of 10 atm to form a transparent KBr pellet. The prepared pellet was analysed by Fourier-transform infrared spectroscopy (FT-IR) using a Perkin Elmer Spectrum Two Fourier Transform Infrared (FT-IR) spectrometer ranging from 400 to 4000 cm^{-1}, employing a resolution of 1 cm^{-1} and averaging 32 scans.

Thermogravimetric analyses were performed by means of Pyris TGA7 (Perkin Elmer, Waltham, MA, USA) in the temperature range between 50 and 800 °C, under an air flow of 60 mL min^{-1} and heating rate of 10 °C min^{-1}.

The measurement and calculation of Cation Exchange Capacity, (CEC) values were performed according to the procedure from ISO 11260:2018 "Soil quality - Determination of effective cation exchange capacity and base saturation level using barium chloride solution". The method is based on saturating the soil's exchange complex with Ba^{2+} ions from a $BaCl_2$ solution. Then, exchangeable cations (Ca^{2+}, Mg^{2+}, K^+, Na^+, and H^+) are displaced by barium. The displaced cations are quantified, and from these data, CEC and base saturation are calculated. All chemical analyses have been replicated three times.

2.2.3. *Preparation and characterization of clay-based suspensions*

Clay-based suspensions were prepared by dispersing the monocationic clay fraction in a hydroalcoholic mixture (water:ethanol =

50:50, v/v) containing resveratrol (RSV; 0.6% (w/w)). Resveratrol was selected as a reference compound owing to its favourable physicochemical characteristics, such as moderate lipophilicity, as well as its well-documented beneficial effects on skin disorders, including inflammation, oxidative stress, and barrier dysfunction [30,31]. The mixture was magnetically stirred at room temperature until complete homogenization (24 h). Each sample was processed under identical conditions to enable a consistent and comparative technological evaluation.

Viscosity was assessed 24 h after sample preparation to ensure complete stabilization of the suspensions. Measurements were conducted using a Brookfield DV-II+ Pro EXTRA rotational viscometer (Brookfield Engineering Laboratories, Inc., Middleboro, MA, USA) equipped with spindle number 6. Prior to analysis, the device was calibrated according to the manufacturer's specifications using silicone oil as the standard reference fluid. Each suspension was transferred into a glass vial and allowed to equilibrate for one hour before testing. Viscosity was recorded at a constant rotational speed of 6, 10, 13, 15, 20 and 25 rpm for 30 s at room temperature. Each sample was measured in triplicate, allowing 5 min between successive readings. Final viscosity values were reported in centipoise (cPs).

Spreadability was assessed using the parallel-plate method with two glass plates (diameter 9 centimetres). One gram of sample was placed between the plates, and a 50 g weight was gently applied on top. After one minute, the weight was removed and the diameter of the spread area was measured in centimetres. Each sample was tested three times.

The pH of the suspensions was measured using a pH meter (Hanna, model HI98103 Checker pH tester), which was previously calibrated with two standard buffer solutions at pH 4.0 and pH 7.0.

The occlusion factor was evaluated following a previously established method. Beakers (100 mL) were filled with 50 mL of distilled water and covered with a cellulose acetate filter. A total of 200 mg of clay-based suspension was evenly spread over the filter surface (18.8 cm^2, equal to 10.6 mg/cm^2). After recording the initial weight, the beakers were placed in an incubator at 37 °C for 24 h, with controlled humidity (60%). At the end of incubation, each beaker was weighed again to determine water loss by evaporation. Identical beakers covered only with filter paper, without formulation, served as the control.

The occlusion factor (F) was calculated using the equation:

$$F = ((A-B)/A) \times 100$$

where A represents water loss from the control beaker and B represents water loss in the presence of the sample. All measurements were performed in triplicate.

In vitro release of RSV from the clay suspensions was evaluated using Franz-type diffusion cells (LGA, Berkeley, CA, USA) [3]. Cellulose membranes were used as the diffusion barrier, selected as a standard, inert and hydrophilic barrier commonly used in in vitro release studies of topical formulations; they provide reproducible separation between donor and receptor compartments without interacting with RSV or clay particles [32,33]. Membranes were pre-hydrated by immersion in distilled water for 1 h at room temperature. Once the membrane was positioned between the donor and receptor compartments, the effective diffusion area was 0.75 cm^2. The donor compartment contained 500 µL of RSV-loaded clay suspension (0.6% w/w RSV, ~3 mg RSV). Since RSV has limited solubility in water, the receptor medium consisted of a water/ethanol mixture (80:20, v/v) to provide sufficient solubility and maintain sink conditions during the experiment. The receptor compartment contained 4.5 mL of this medium, maintained at 35 °C and stirred at 700 rpm so that the surface in contact with the membrane remained at 32 °C throughout the experiment. Sink conditions were considered maintained because the total RSV applied in the donor (~3 mg) is well below its solubility in the receptor medium [34], preventing saturation during the 24 h experiment. At 24 h, 200 µL of receptor medium was withdrawn and RSV content was quantified by UV-Vis spectrophotometry (Shimadzu UV-1601, Shimadzu Italia, Milan, Italy) at its $\lambda_{max=}$ 306 nm. A calibration curve was generated in the range 1–10 µg/mL using the same hydroalcoholic medium (R^2= 0.99978). All experiments were carried out in triplicate and data were processed as mean ± SD.

3. Results

3.1. Bulk mineralogical and chemical characterization

Table 1 listed the results of XRF analysis of the four deposits. In detail, the chemical analysis evidenced a silica-alumina rich composition for all deposits, with $SiO_2 + Al_2O_3$ sum accounting for about three-quarters of the bulk composition (65–74 wt%). Two clusters concerning the alumina and iron contents were defined: higher values in CALT deposits than those of SIL and CEN samples. Instead, the highest CaO amount (6.81 wt%) among the four samples was recorded in SIL, while the lowest for CALT2 (0.42 wt%). However, this latter recorded the highest combined alkali content ($Na_2O + K_2O$ = 3.49 wt%) and the lowest LOI (7.72 wt%), confirming a low-carbonate matrix. Moreover, the narrow range in TiO_2 (0.79–1.21 wt%) and P_2O_5 (0.15–0.18 wt%) values suggest that these elements are due to negligible accessory phases. Overall, the four deposits can be regarded as broadly similar, with a distinctive chemical fingerprint (especially for the trace/minor elements) that could influence both processing behaviour and end-use performance. These minor disparities suggest different geological contexts and will need to be weighed carefully in any topical application where specific heavy-metal ceilings apply. The ICP-MS dataset reveals clear geochemical contrasts among the four sampling sites (SIL, CEN, CALT1 and CALT2). Major elements show the most pronounced variability: Mg ranges from ~13,800 ppm in CALT2 to over 19,000 ppm in CEN, while Fe spans from ~41,900 ppm (CEN) to more than 69,000 ppm in CALT2, marking this site as particularly enriched in iron.

Table 1
- Concentrations of major (wt%) and minor/trace (in ppm) elements determined by XRF analysis of sampled deposits (first block); Loss on ignition (LOI); ICP-MS elemental concentrations (in ppm) of some major and trace elements measured in the four clay samples (second block; n.d. not determined because below detection limit).

	SIL	CEN	CALT1	CALT2
SiO_2	50.24	51.91	46.63	54.15
TiO_2	0.82	0.79	0.89	1.21
Al_2O_3	16.58	16.49	18.76	19.93
Fe_2O_3	6.54	6.20	11.42	10.46
CaO	6.81	5.65	4.98	0.42
Na_2O	0.46	1.32	1.05	1.43
K_2O	1.92	2.31	1.64	2.06
P_2O_5	0.15	0.15	0.17	0.18
LOI	13.27	11.74	10.90	7.72
Rb	93	107	68	86
Y	24	24	24	26
Zr	201	160	118	170
Nb	18	15	14	22
Mg	16271	19064	14426	13791
V	187	171	357	365
Cr	147	136	248	230
Mn	310	79	439	96
Fe	48318	41860	48165	69218
Co	13.17	7.69	19.31	17.25
Ni	49.99	41.03	58.04	58.60
Cu	32.21	38.72	48.94	33.09
Ti	3202	908	6537	8150
Zn	168	111	124	124
As	9.36	2.10	1.94	1.28
Se	1.82	1.21	1.78	2.23
Sr	123	29	235	185
Cd	n.d.	n.d.	n.d.	n.d.
Sb	n.d.	n.d.	n.d.	n.d.
Ba	123	41	158	142
Pb	18.29	8.20	21.43	23.03

Manganese also exhibits striking differences, with CALT1 showing the highest concentration (~439 ppm) and CALT2 and CEN substantially lower values (<100 ppm). Among the transition metals, V and Cr follow similar patterns, being consistently higher in the CALT samples, while CEN and SIL display markedly reduced concentrations. Trace metals such as Co, Ni, Cu, and Zn vary more moderately but still tend to be elevated in the CALT sites. Moreover, selenium shows the strongest divergence, reaching its maximum at CALT1 (~6.3 ppm), while remaining below 1 ppm in the other samples. Ba and Sr are substantially higher at SIL and CALT1, with Ba peaking at SIL (~503 ppm) and Sr at CALT1 (~334 ppm). Elements such as As, Cd, Pb and U remain uniformly low across all sites, indicating no significant enrichment in any specific location. Moreover, in accordance with Article 17 of Regulation (EC) No. 1223/2009, the clay's safety profile is guaranteed by heavy metal concentrations that do not exceed the technically unavoidable thresholds set out in the Italian ISS, the German BVL and the European Pharmacopoeia. This confirms that these clays can be used for topical studies. Overall, the CALT1 and CALT2 samples are characterized by elevated concentrations of several major and trace metals (particularly Fe, Mg, V, Cr, Mn, Se), whereas CEN consistently exhibits the lowest elemental abundances. SIL stands out mainly for its high Ba and moderately elevated Mg and Fe values. These patterns point to distinct geochemical signatures and potential differences in source materials or environmental processes governing each site.

Fig. 2 overlapped the XRD patterns of the bulk deposits, while Table 2 reported the amount of non-clay and clay minerals (CM). All samples were made of mixed mineral assemblages where CM represent the dominant fraction (53–68 wt%), associated with variable amounts of quartz (17–23 wt%), feldspar (7–16 wt%) and calcite (1–9 wt%), with few gypsums and hematite detected only in CALT2 (2.4 wt%). Among phyllosilicates, smectite, interlayered smectite/illite, kaolinite and illite were identified. The presence of mixed-layer I/S in CEN and CALT2

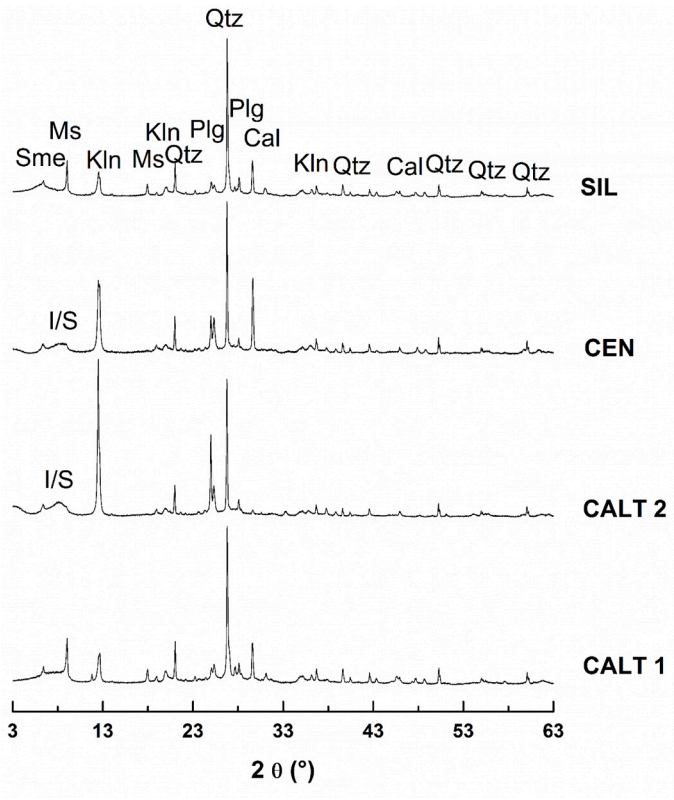

Fig. 2. XRD patterns of bulk deposits. Legenda: I/S = interlayered smectite/illite; Ms = illite/muscovite; Kln = kaolinite; Plg = plagioclase; Qtz = quartz; Sme = smectite.

Table 2 –
Summary of qualitative analysis of bulk samples. The abundances are expressed in wt%. Legenda: CM = clay minerals (i.e., chamosite, chlorite, illite, kaolinite and smectite).

	CM	calcite	feldspar	gypsum	hematite	quartz
SIL	52.9	8.6	16.3	0.5	0.0	21.8
CEN	63.8	6.2	7.5	0	0	22.5
CALT1	68.0	6.1	7.3	1.1	0	17.6
CALT2	56.5	1.3	16.0	0.9	2.4	23.0

indicates a progressive illitisation of smectite. Overall, these bulk data provide the mineralogical context of the raw deposits, whereas the detailed identification and relative abundance of individual clay phases were resolved by focusing on the mineralogy of ≤ 2 μm clay fraction.

3.2. PSD, mineralogical, spectroscopic and thermal characterization

Laser diffraction analysis of the < 32 μm fraction revealed measurable differences in particle-size distribution among the investigated samples (Table 3). SIL showed the coarsest distribution (d50 = 8.46 μm; d90 = 21.72 μm), whereas CEN and the CALT samples were finer, with d50 values of 6.14 μm (CEN), 5.73 μm (CALT1) and 5.57 μm (CALT2), and d90 values ranging from 15.15 to 16.81 μm. The d10 values were 1.62 μm (SIL), 1.72 μm (CEN), 1.34 μm (CALT1) and 1.33 μm (CALT2), indicating a slightly higher proportion of the finest particles in the CALT samples compared with SIL and CEN. Fig. 3 showed the patterns collected on clay fractions (<2 μm) after three common laboratory treatments: air-drying (AD), swelling with ethylene glycol (EG) and heating to 375 °C (T375). In SIL and CEN, the main clay peak moved from about ~ 6–8° 2θ in the air-dried state to 5° after glycolation, then shifted back toward ~ 9° when heated (Fig. 3a-b). This expand-collapse behaviour revealed a smectite-rich illite/smectite mixture that can take up water (or glycol) between its layers and lose it on heating; small, sharp peaks at ~ 12° confirmed a minor amount of kaolinite in addition to that of illite/smectite mixture with about 80% of illite (I/S80R0). Instead, the other two samples, belonging to the same geological formation, namely CALT1 and CALT2, behaved differently (Fig. 3c-d). Their principal peak settled at a clearer 9° 2θ position after heating, showing that these clays contain illite layers, namely I/S75R1. In detail, CALT1 also displayed a fixed peak at 6° that never moves, pointing to the presence of chlorite, a mineral that neither swells nor collapses under the tests applied. Table 2 indicated the relative amounts of all mineral phases detected for each sample and the measured cation exchange capacity (CEC). Despite the clay quantification is challenging [35], from the comparison of all patterns, the samples can be clustered into two families: SIL and CEN richer in pure smectite (6 and10 wt% respectively) and kaolinite (24 and 34 wt% respectively) than CALT1 and CALT2 clays (Table 3). However, these latter evidenced a higher number of illite/smectite interlayers (80 and 93 wt% respectively) than the first cluster. Therefore, the overall sum of expandable clay minerals is higher

Table 3 –
Particle size distribution (PSD) descriptors of the < 32 μm fraction measured by laser diffraction. Values are reported as d10, d50 and d90 in μm. Summary of qualitative and semiquantitative analysis on EG slides of clay fractions (<2 μm). The abundances are expressed in wt%. Cation exchange capacity (CEC) of the clay samples is measured in cmol·kg^{-1}.

	SIL	CEN	CALT1	CALT2
d90	21.72	15.46	16.81	15.15
d50	8.46	6.14	5.73	5.57
d10	1.62	1.72	1.34	1.33
Kaolinite	34.5	24.6	8.6	6.5
Illite/Smectite	54.9	63.1	80.6	93.5
Smectite	10.7	6.2	-	-
Chlorite	-	6.1	10.8	-
CEC	26.88	26.29	21.46	20.32

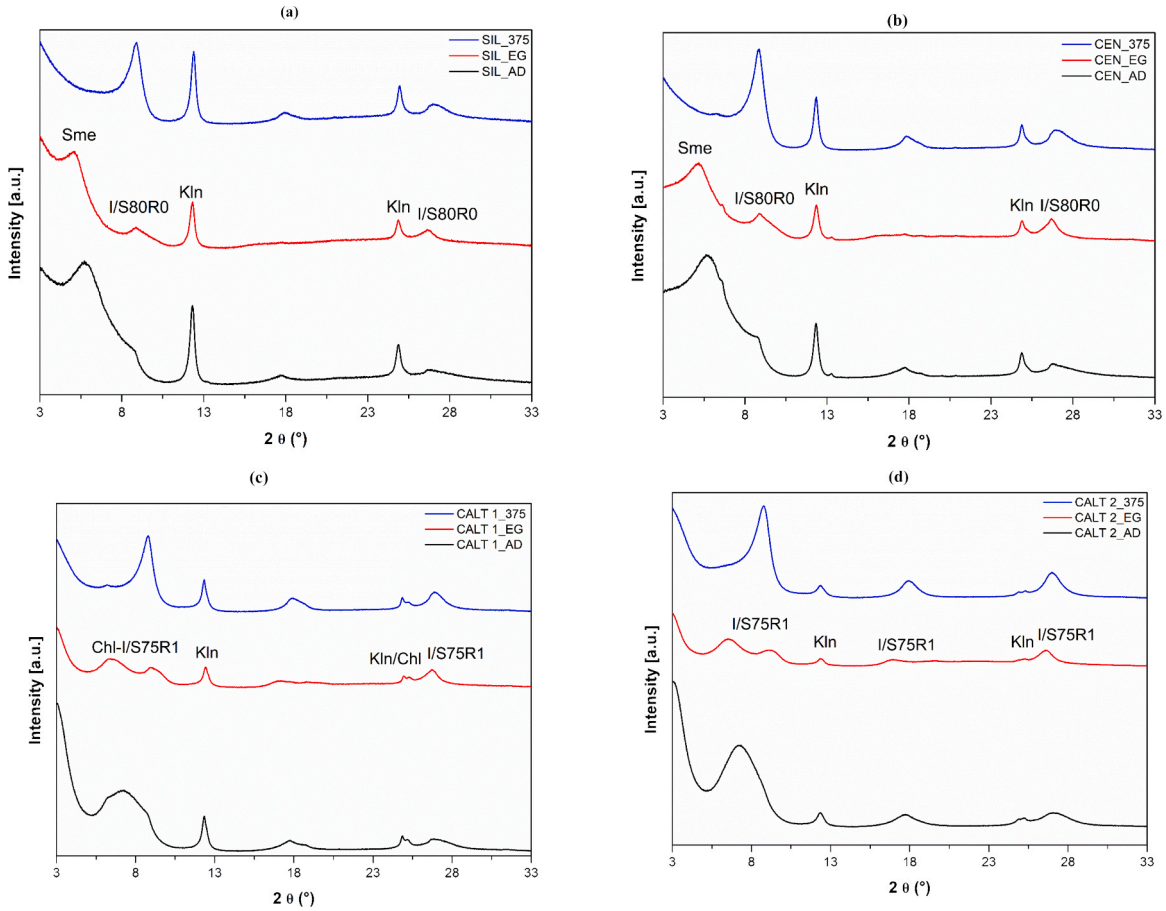

Fig. 3. Overlap of XRD patterns of the slides with the clay fractions of (a) SIL, (b) CEN, (c) CALT1 and (d) CALT2 in different conditions: AD = air dried (black line); EG = ethylene glycol (red line); 375 = thermal treatment at 375°C (blue line). Legenda: I/S = interlayered illite/smectite ratio; Chl = chlorite; Kln = kaolinite; Sme = smectite. R indicates the ordering levels: R = 0 (disordered), R= 1 (partially ordered), and R= 2 (ordered) (Moore and Reynolds, 1997).

in CALT set. Regarding the CEC, no significant difference was observed among the all samples. However, the clay fraction (< 2 μm) with the highest cation exchange capacity was SIL (26.88 cmol·kg^{-1}), followed by CEN (26.29 cmol·kg^{-1}) and CALT1 and CALT2 (21.46 cmol·kg^{-1} and 20.32 cmol·kg^{-1}) respectively (Table 3). This trend can be explained by considering that SIL contains the highest proportion of pure smectite of all the clay samples.

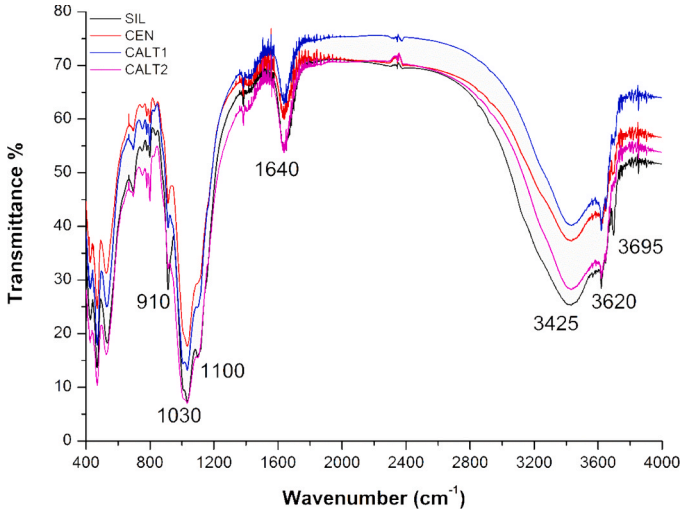

Fig. 4. Overlap of FTIR spectra of the clay samples in the 400–4000 cm^{-1} range (spatial resolution of 1 cm^{-1}).

Fig. 4 displays the overlapped FT-IR spectra of the four clay fractions. The broad O–H-stretch envelope centred at ~3425 cm^{-1}, together with H_2O-bending band at 1640 cm^{-1}, is noticeably deeper for SIL and CALT2 than for CALT1 and CEN, suggesting that the former pair hosts more interlayer water-consistent. Within the structural -OH region, the same trend was observed at 3620 cm^{-1}, confirming internal hydroxyl groups in all clay samples. Instead, the distinct band at 3695 cm^{-1}, more evident in SIL, indicates higher kaolinite content, as it corresponds to Al–OH stretching vibrations, also confirmed by 910 cm^{-1} peak. The peaks at 1030 and 1100 cm^{-1} are related to the stretching vibration of the Si-O bonds, characteristic of clay samples [36].

Thermogravimetric analysis was performed to evaluate the thermal decomposition behaviour and to qualify and quantify the water content of the clay samples. The TGA profiles illustrated in Fig. 5 reveal a multi-stage weight loss for each sample as a function of increasing temperature. The loss weight starting below 100 °C is caused by the evaporation of adsorbed water on the external surfaces of the clay particles and within the larger pores. In detail, the SIL and CEN samples demonstrate a more pronounced initial decline at 100°C, with respective losses of approximately 7% and 5%, suggesting a high level of adsorbed water. On the other hand, the CALT 1 and CALT 2 show minimal loss (approximately 3% of weight), indicating a lower content of adsorbed water. The most significant weight loss for the clay samples (i.e., about 5%) is observed in the temperature range of approximately 400–600 °C. This major event corresponds to the dehydroxylation of the clay minerals, specifically the removal of structural hydroxyl groups (-OH). At temperatures above 600 °C, the TGA curves show less pronounced

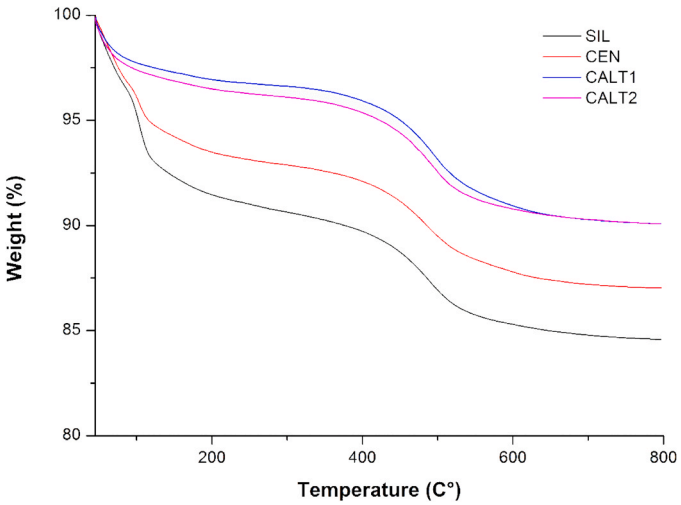

Fig. 5. Thermal decomposition of clay samples.

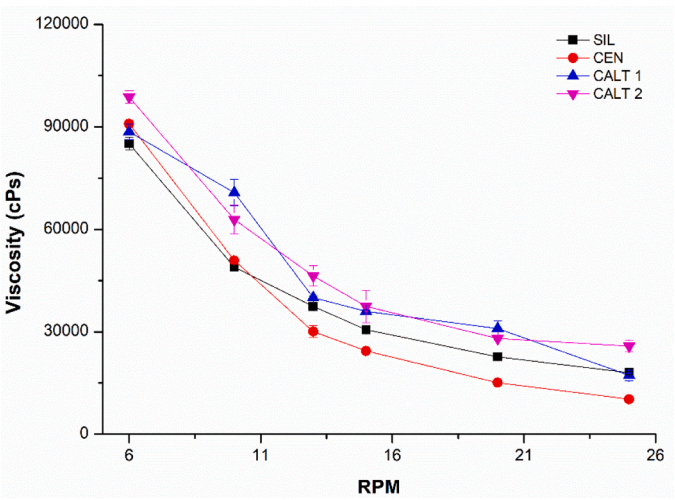

Fig. 6. Viscosity measurements of SIL, CEN, CALT1 and CALT2 suspensions as a function of rotational speed (RPM). Data are presented as mean ± SD (n = 3).

weight loss events. These can be attributed to the decomposition of other mineral impurities such as carbonates (e.g., calcite or dolomite), which release carbon dioxide (CO_2) upon thermal degradation [37,38]. The distinct weight loss steps and their corresponding temperatures and magnitudes on the TGA curves serve as a unique thermal fingerprint for each clay sample. The significant differences observed between the CALT samples and the CEN and SIL samples suggest a substantial variation in their mineralogical composition. In summary, SIL is the least thermally stable, with a total mass loss of 15.5%, while the CALT clays are the most robust.

3.3. *Characterization of clay-based suspensions*

The results of all four clay-based suspensions, prepared with particle sizes ≤ 2 μm dispersed in a 50:50 hydro-alcoholic solution containing 0.6% RSV, are listed in Table 4. In detail, they exhibited a neutral pH between 6.5 and 7, suitable for topical application. Viscosity values determined at 6 rpm showed slight variations depending on the clay type, ranging from 85.08 ± 1.92 cPs for SIL to 98.75 ± 1.58 cPs for CALT2. Viscosity measurements of all clay-suspensions as a function of rotational speed displayed similar trends as an analogous drop of viscosity was observed for all formulations by increasing the rotational speed (Fig. 6). Spreadability measurements revealed that CALT1 suspension was less easily spread (3.5 ± 0.58 cm) compared to SIL (6.40 ± 0.25 cm), CEN (5.00 ± 0.04 cm) and CALT2 (5.00 ± 0.10 cm), indicating higher resistance to spreading for the CALT1 clay. The occlusion factor was higher for CALT1 and CALT2 (38.46 ± 0.13% and 40.07 ± 0.05%, respectively) than for SIL and CEN (35.74 ± 0.03% and 37.50 ± 0.03%), suggesting a greater potential for forming a protective film on the skin. A preliminary release study was conducted using vertical Franz diffusion cells for 24 h with an ethanol:water (20:80) receptor medium. The RSV release differed depending on the clay used: CALT1 exhibited the highest release at 22.28 ± 0.003%, followed by CALT2 at 17.32 ± 0.01%, SIL at 16.34 ± 0.25% and CEN at 7.52 ± 0.03%. All experiments were carried out in duplicate, and the low variability among replicates indicates that the measurements were highly reproducible. Therefore, these findings indicate that key technological properties of the suspensions (viscosity, spreadability and occlusive capacity) are influenced by the mineralogical nature of the clays used.

Table 4
pH, viscosity, spreadability, occlusion factor, and release percentage of the four clay samples (SIL, CEN, CALT1 and CALT2).

	SIL	CEN	CALT 1	CALT 2
pH	7.0	7.0	6.5	7.0
Viscosity (cPs)	85.083 ± 1.916	90.917 ± 2.503	88.583 ± 2.250	98.750 ± 1.583
Spreadability (cm)	6.4 ± 0.252	5.0 ± 0.041	3.5 ± 0.577	5.0 ± 0.100
Occlusion Factor (%)	35.74 ± 0.034	37.5 ± 0.031	38.46 ± 0.134	40.07 ± 0.053
Percentage Cumulative (%)	16.34 ± 0.245	7.52 ± 0.032	22.28 ± 0.003	17.32 ± 0.005

4. Discussion

The chemical, mineralogical and structural characterization of four clay deposits revealed significant differences beyond simple geochemical variability. CALT1 and CALT2 were richer in alumina and iron and contained higher proportions of interlayered illite/smectite (I/S), with CALT1 also containing chlorite, whereas SIL and CEN were relatively richer in smectite and kaolinite. These compositional and structural variations, rather than particle size alone, influence the functional properties of the clay fractions [39]. Laser diffraction on the < 32 μm fraction indicates that SIL has the coarsest PSD, whereas CEN and the CALT samples are finer overall. In particular, CALT samples show a slightly higher contribution of the finest particles. The ≤ 2 μm fractions preserve the key phyllosilicate structures while minimizing coarse, non-clayey minerals, ensuring better dispersion, uniformity and reproducible rheology. The clay-resveratrol suspensions investigated in this study should be regarded as simplified pre-formulation models rather than finished cosmetic products. They allow a controlled comparison of how mineralogical features influence technological properties and release behaviour under identical experimental conditions. While industrial cosmetic applications often rely on highly purified mono-mineralic clays [40], mixed natural assemblages may offer sustainable, locally available alternatives, provided that fine fractions are selected and chemical safety requirements are met. Natural clays may show batch-to-batch compositional variability: therefore, any future industrial use would require standardized sampling procedures, together with routine mineralogical quality control to ensure reproducibility [41,42]. CALT1 and CALT2 fractions, with abundant I/S layers and limited swelling, are expected to form cohesive, stable films on the skin. In contrast, SIL and CEN fractions, richer in smectite and kaolinite, offer higher water retention and cation exchange capacity but lower structural rigidity. These characteristics render the fine fractions particularly relevant for topical delivery systems and skin-contact applications [39], with CALT1 and CALT2 standing out for their structural stability, low carbonate content and favourable trace element profiles. Based on these considerations, resveratrol (0.6% RSV) was selectively loaded onto the

≤ 2 μm fractions dispersed in a 50:50 hydro-alcoholic medium to assess the impact of clay type on bioactive delivery. All RSV-suspensions exhibited a neutral pH (6.5–7), suitable for topical application and skin barrier maintenance [43]. CALT-based suspensions displayed higher occlusion factors and lower spreadability compared to SIL and CEN, indicating that the rigid I/S layers favour cohesive, stable film formation rather than easy spreading. Interestingly, no direct correlation was observed between viscosity and spreadability, suggesting that intrinsic structural properties of the clay matrix, rather than fluid density, govern mechanical resistance and occlusion. Overall, PSD differences may contribute to suspension behaviour; however, the distinct mineralogical assemblages support mineralogy and microstructure as major drivers of the observed functional trends. Rheological profiles across varying rotational speeds further supported this interpretation, with CALT1 and CALT2 showing similar behaviour consistent with a rigid, deformation-resistant structure, whereas SIL and CEN followed distinct but internally consistent trends [44]. A preliminary release study using vertical Franz diffusion cells over 24 h in an ethanol:water (20:80) receptor medium demonstrated that RSV release varied depending on the clay type: CALT1 exhibited the highest release (22.28 ± 0.003%), followed by CALT2 (17.32 ± 0.005%), SIL (16.34 ± 0.245%) and CEN (7.52 ± 0.032%). These differences reflect the structural and mineralogical characteristics of the clays. Clay formulations rich in illite/smectite interlayers (CALT1 and CALT2) showed higher RSV release, likely due to their larger interlayer spacing, rigid microstructure and limited swelling, which facilitate drug desorption and diffusion [45]. In contrast, kaolinite-rich systems (SIL and CEN), with lower surface area and non-expandable layers, exhibited slower release, although factors such as water retention and cation exchange capacity can modulate diffusion [46]. Although limited to 24 h, these trends align with previous reports indicating that smectite-rich clays can release more active compounds than kaolinite-based ones. Overall, these preliminary results suggest that smectite-rich clays could be promising carriers for enhanced and sustained RSV delivery [47,48]. Mineralogical composition and microstructure, together with particle-size distribution and surface-related properties, appear to be key factors influencing release behaviour and overall suspension performance. In particular, CALT1 and CALT2 combine structural stability, favourable trace element profiles and functional performance, making them interesting candidates for further investigation in topical applications.

5. Conclusion

This study highlights how the mineralogical and microstructural features of natural clays strongly influence their behaviour in topical delivery of resveratrol. By focusing on the fine (≤ 2 μm) fractions, the intrinsic properties of the clays could be evaluated in a reproducible way, allowing a clear comparison of their functional performance. Among the investigated Sicilian clays, CALT1 and CALT2 showed the most promising behaviour, forming more occlusive dispersions and supporting a higher and more sustained release of resveratrol. In contrast, SIL and CEN, although characterized by higher water retention, displayed a lower release efficiency. These differences underline that mineralogical structure, rather than simple parameters such as particle size or viscosity, plays a key role in controlling formulation performance. Nevertheless, PSD indicates slight differences in particle-size distribution that may act as a secondary contributing factor to suspension behaviour. This study establishes a material-oriented pre-formulation framework for selecting natural clay carriers based on fine-fraction mineralogy and functional screening, supporting Sicilian clays as sustainable candidates for topical applications. Future work should address long-term physicochemical stability, advanced release kinetics, in vitro skin permeation and comprehensive safety/regulatory evaluation to optimize resveratrol delivery and support the development of effective topical products.

CRediT authorship contribution statement

Lucia Montenegro: Writing – review & editing, Validation, Supervision, Methodology, Data curation, Conceptualization. **Giuseppe Maccarrone:** Validation, Supervision, Software, Methodology. **Salvatore Barreca:** Writing – original draft, Investigation, Formal analysis, Data curation. **Paolo Mazzoleni:** Writing – review & editing, Validation, Supervision, Software, Resources, Project administration, Methodology, Funding acquisition, Data curation, Conceptualization. **Antonino Chindemi:** Investigation, Formal analysis. **Rosario Pignatello:** Writing – review & editing, Validation, Supervision, Resources, Project administration, Methodology, Funding acquisition, Conceptualization. **Carmelo Puglia:** Writing – review & editing, Validation, Supervision, Methodology, Conceptualization. **Debora Santonocito:** Writing – review & editing, Writing – original draft, Validation, Methodology, Investigation, Formal analysis, Data curation, Conceptualization. **Claudio Finocchiaro:** Writing – review & editing, Writing – original draft, Visualization, Methodology, Investigation, Formal analysis, Data curation, Conceptualization. **Germana Barone:** Writing – review & editing, Validation, Supervision, Software, Methodology, Investigation, Conceptualization.

Declaration of Competing Interest

The authors declare that they have no known competing financial interests or personal relationships that could have appeared to influence the work reported in this paper.

Acknowledgments

The authors wish to thank dr. Salvatore Distefano for performing the particle-size distribution (PSD) of the < 32 μm fraction, Mrs Michelangelo Sapienza and Salvatore Risiglione for their precious help during the grain size separations of clay deposits. This research was supported by "PIAno di inCEntivi per la RIcerca di Ateneo (PIA.CE.RI. 2024/2026) of the University of Catania - UPB 57722172154.

Data Availability

Data will be made available on request.

References

[1] F. Wypych, R.A. de Freitas, Clay minerals: classification, structure, and properties, Dev. Clay Sci. 10 (2022) 3–35, https://doi.org/10.1016/B978-0-323-91858-9.00004-5.
[2] N. Kumari, C. Mohan, N. Kumari, C. Mohan, Basics of clay minerals and their characteristic properties, Clay Clay Miner. (2021), https://doi.org/10.5772/intechopen.97672.
[3] F.P. Bonina, M.L. Giannossi, L. Medici, C. Puglia, V. Summa, F. Tateo, Adsorption of salicylic acid on bentonite and kaolin and release experiments, Appl. Clay Sci. 36 (2007) 77–85, https://doi.org/10.1016/j.clay.2006.07.008.
[4] M. Massaro, C.G. Colletti, G. Lazzara, S. Riela, The use of some clay minerals as natural resources for drug carrier applications, J. Funct. Biomater. 9 (4) (2018) 58, https://doi.org/10.3390/jfb9040058.
[5] J.D.D. Moraes, S.R.A. Bertolino, S.L. Cuffini, D.F. Ducart, P.E. Bretzke, G. R. Leonardi, Clay minerals: Properties and applications to dermocosmetic products and perspectives of natural raw materials for therapeutic purposes—a review, Int. J. Pharm. 534 (2017) 213–219, https://doi.org/10.1016/j.ijpharm.2017.10.031.
[6] B.O. Otunola, O.O. Ololade, A review on the application of clay minerals as heavy metal adsorbents for remediation purposes, Environ. Technol. Innov. 18 (2020) 100692, https://doi.org/10.1016/j.eti.2020.100692.
[7] M.I. Carretero, M. Pozo, Clay and non-clay minerals in the pharmaceutical and cosmetic industries Part II. Active ingredients, Appl. Clay Sci. 47 (2010) 171–181, https://doi.org/10.1016/j.clay.2009.10.016.
[8] C. Finocchiaro, G. Barone, P. Mazzoleni, G. Spagnolo, New insights on the archaic 'Corinthian B' amphorae from Gela (Sicily): The contribution of the analyses of Corfu raw materials, Mediterr. Archaeol. Archaeom. 18 (2018) 179–189, https://doi.org/10.5281/zenodo.1285908.
[9] F. Lentini, S. Carbone, Geology of Sicily. Periodici tecnici, Mem. Descr. della Carta Geol. D. 'Ital. (2014). ISSN: 0536-0242.

[10] A. Di Grande, V. Giandinoto, Plio-Pleistocene sedimentary facies and their evolution in centre-south-eastern Sicily: a working hypothesis, Stephan. Mueller Spec. Publ. Ser. 1 (2002) 211–221, https://doi.org/10.5194/smsps-1-211-2002.
[11] G. Barone, P. Mazzoleni, G.V. Spagnolo, S. Raneri, Artificial neural network for the provenance study of archaeological ceramics using clay sediment database, J. Cult. Herit. 38 (2019) 147–157, https://doi.org/10.1016/j.culher.2019.02.004.
[12] G. Barbera, S. Critelli, P. Mazzoleni, Petrology and geochemistry of Cretaceous sedimentary rocks of the Monte Soro Unit (Sicily, Italy): constraints on weathering, diagenesis, and provenance, J. Geol. 119 (2011) 51–68, https://doi.org/10.1086/657340.
[13] G. Montana, M.Á. Cau Ontiveros, A.M. Polito, E. Azzaro, Characterisation of clayey raw materials for ceramic manufacture in ancient Sicily, Appl. Clay Sci. 53 (2011) 476–488, https://doi.org/10.1016/j.clay.2010.09.005.
[14] A. Stroscio, G. Barone, A. Fernàndez-Jimenez, I. Lancellotti, C. Leonelli, P. Mazzoleni, Sicilian clay sediments as precursor for alkali activated materials, Appl. Clay Sci. 253 (2024) 107350, https://doi.org/10.1016/j.clay.2024.107350.
[15] C. Viseras, C. Aguzzi, P. Cerezo, A. Lopez-Galindo, Uses of clay minerals in semisolid health care and therapeutic products, Appl. Clay Sci. 36 (2007) 37–50, https://doi.org/10.1016/j.clay.2006.07.006.
[16] C. Viseras, P. Cerezo, R. Sanchez, I. Salcedo, C. Aguzzi, Current challenges in clay minerals for drug delivery, Appl. Clay Sci. 48 (2010) 291–295, https://doi.org/10.1016/j.clay.2010.01.007.
[17] C. Roselli, D. Desideri, C. Cantaluppi, M. Mattioli, A. Fasson, M.A. Meli, Essential and toxic elements in clays for pharmaceutical and cosmetic use, J. Toxicol. Environ. Health A 78 (2015) 316–324, https://doi.org/10.1080/15287394.2014.964430.
[18] A. López-Galindo, C. Viseras, P. Cerezo, Compositional, technical and safety specifications of clays to be used as pharmaceutical and cosmetic products, Appl. Clay Sci. 36 (2007) 51–63, https://doi.org/10.1016/j.clay.2006.06.016.
[19] M.I. Carretero, M. Pozo, Clay and non-clay minerals in the pharmaceutical industry: Part I. Excipients and medical applications, Appl. Clay Sci. 46 (2009) 73–80, https://doi.org/10.1016/j.clay.2009.07.017.
[20] B.H. Rao, P.S. Reddy, B. Mohanty, K.R. Reddy, Combined effect of mineralogical and chemical parameters on swelling behaviour of expansive soils, Sci. Rep. 11 (2021) 1–20, https://doi.org/10.1038/S41598-021-95746.
[21] M. Jafarbeglou, M. Abdouss, A.M. Shoushtari, M. Jafarbeglou, Clay nanocomposites as engineered drug delivery systems, RSC Adv. 6 (2016) 50002–50016, https://doi.org/10.1039/C6RA03942A.
[22] J. de Carvalho Arjona, C. Ulsen, F.R. Valenzuela-Diaz, N.R. Demarquette, Influence of smectite clays' pores volume on isoniazid adsorption and release, Appl. Clay Sci. 252 (2024) 107341, https://doi.org/10.1016/j.clay.2024.107341.
[23] M. Henriquet, S. Dominguez, G. Barreca, J. Malavieille, C. Monaco, Structural and tectono-stratigraphic review of the Sicilian orogen and new insights from analogue modeling, Earth. Sci. Rev. 208 (2020) 103257, https://doi.org/10.1016/j.earscirev.2020.103257.
[24] I.R. Finetti, F. Lentini, S. Carbone, A. Del Ben, A. Di Stefano, E. Forlin, P. Guarnieri, M. Pipan, A. Prizzon, Geological outline of Sicily and lithospheric tectono-dynamics of its Tyrrhenian margin from new CROP seismic data, 2005, pp. 319–375. ⟨https://pub.geus.dk/en/publications/geological-outline-of-sicily-and-lithospheric-tectono-dynamics-of⟩ (accessed June 24, 2025).
[25] M. Grasso, H. Martyn Pedley, The sedimentology and development of Terravecchia Formation carbonates (Upper Miocene) of North Central Sicily: Possible eustatic influence on facies development, Sediment. Geol. 57 (1988) 131–149, https://doi.org/10.1016/0037-0738(88)90022-X.
[26] S. Raneri, R. Torre, P. Mazzoleni, C. Portale, G. Barone, From βαλανεῖα to thermae: unveiling the transition from Greek to Roman architectural models of baths by technological and provenance archaeometric studies on bricks and tiles, ArcheoSciences 43 (2019) 187–202, https://doi.org/10.4000/archeosciences.6686.
[27] N. Doebelin, R. Kleeberg, Profex: A graphical user interface for the Rietveld refinement program BGMN, J. Appl. Crystallogr 48 (2015) 1573–1580, https://doi.org/10.1107/S1600576715014685.
[28] D.M. Moore, R.Jr Reynolds, X-ray Diffraction and the Identification and. Analysis of Clay Minerals, second, Oxford University Press, Oxford, 1997.
[29] R. Reynolds, NEWMOD, a Computer Program for the Calculation of One-Dimensional Diffraction Patterns of Mixed-Layered Clays. 8 Brook Road, Hanover, NH, 03755.
[30] M.H. Lin, C.F. Hung, H.C. Sung, S.C. Yang, H.P. Yu, J.Y. Fang, The bioactivities of resveratrol and its naturally occurring derivatives on skin, J. Food Drug Anal. 29 (2021) 15–38, https://doi.org/10.38212/2224-6614.1151.
[31] M. Marko, R. Pawliczak, Resveratrol and its derivatives in inflammatory skin disorders—atopic dermatitis and psoriasis: a review, Antioxidants 12 (2023) 1954, https://doi.org/10.3390/antiox12111954.
[32] A. Simon, M.I. Amaro, A.M. Healy, L.M. Cabral, V.P. de Sousa, Comparative evaluation of rivastigmine permeation from a transdermal system in the Franz cell using synthetic membranes and pig ear skin with in vivo-in vitro correlation, Int. J. Pharm. 512 (2016) 234–241, https://doi.org/10.1016/j.ijpharm.2016.08.052.
[33] E. Pena-Rodríguez, M. Lajarin-Reinares, A. Mata-Ventosa, S. Pérez-Torras, F. Fernández-Campos, Dexamethasone-loaded lipomers: development, characterization, and skin biodistribution studies, Pharmaceutics 13 (2021) 533, https://doi.org/10.3390/pharmaceutics13040533.
[34] K. Robinson, C. Mock, D. Liang, Pre-formulation studies of resveratrol, Drug Dev. Ind. Pharm. 41 (2015) 1464–1469, https://doi.org/10.3109/03639045.2014.958753.
[35] X. Zhou, D. Liu, H. Bu, L. Deng, H. Liu, P. Yuan, P. Du, H. Song, XRD-based quantitative analysis of clay minerals using reference intensity ratios, mineral intensity factors, Rietveld, and full pattern summation methods: a critical review, Solid Earth Sci. 3 (2018) 16–29, https://doi.org/10.1016/j.sesci.2017.12.002.
[36] A. Kumar, P. Lingfa, Sodium bentonite and kaolin clays: comparative study on their FT-IR, XRF, and XRD, Mater. Today Proc. 22 (2020) 737–742, https://doi.org/10.1016/j.matpr.2019.10.037.
[37] J.M. Valverde, A. Perejon, S. Medina, L.A. Perez-Maqueda, Thermal decomposition of dolomite under CO2: insights from TGA and in situ XRD analysis, Phys. Chem. Chem. Phys. 17 (2015) 30162–30176, https://doi.org/10.1039/C5CP05596B.
[38] C. Rodriguez-Navarro, E. Ruiz-Agudo, A. Luque, A.B. Rodriguez-Navarro, M. Ortega-Huertas, Thermal decomposition of calcite: mechanisms of formation and textural evolution of CaO nanocrystals, Am. Mineral. 94 (2009) 578–593, https://doi.org/10.2138/AM.2009.3021.
[39] C. Viseras, E. Carazo, A. Borrego-Sánchez, F. García-Villén, R. Sánchez-Espejo, P. Cerezo, C. Aguzzi, Clay minerals in skin drug delivery, 2019 67:1, Clays Clay Miner. 67 (2019) 59–71, https://doi.org/10.1007/S42860-018-0003-7.
[40] M.I. Carretero, M. Pozo, Clay and non-clay minerals in the pharmaceutical and cosmetic industries Part II. Active ingredients, Appl. Clay Sci. 47 (2010) 171–181, https://doi.org/10.1016/j.clay.2009.10.016.
[41] S.R. Obireddy, C. Yu, Q. Zhang, W.F. Lai, D. Zhang, Development and biomedical use of clay-based nanoparticulate systems: recent advances and future directions, Mater. Des. 259 (2025) 114934, https://doi.org/10.1016/j.matdes.2025.114934.
[42] R. Nisticò, A comprehensive study on the applications of clays into advanced technologies, with a particular attention on biomedicine and environmental remediation, Inorganics 10 (2022), https://doi.org/10.3390/inorganics10030040.
[43] S. Hawkins, B.R. Dasgupta, K.P. Ananthapadmanabhan, Role of pH in skin cleansing, Int. J. Cosmet. Sci. 43 (2021) 474–483, https://doi.org/10.1111/ICS.12721.
[44] J.D. Shultz, G.R. Leonardi, S.R.A. Bertolino, S.L. Cuffini, H. Mohd, A.C. Caritá, W. Luiz-Silva, P. Shah, W.G.T. Chambi, B. Michniak-Kohn, Design and development of raw clay-based formulations emulsions loaded with ascorbyl glucoside, in vitro evaluations on topical delivery and cell viability, J. Dispers. Sci. Technol. 45 (2024) 731–742, https://doi.org/10.1080/01932691.2023.2178452.
[45] F. Deon, F. van Ruitenbeek, H. van der Werff, M. van der Meijde, C. Marcatelli, Detection of interlayered illite/smectite clay minerals with XRD, SEM analyses and reflectance spectroscopy, Sensors 22 (2022), https://doi.org/10.3390/S22093602.
[46] L.A. de S. Rodrigues, A. Figueiras, F. Veiga, R.M. de Freitas, L.C.C. Nunes, E.C. da Silva Filho, C.M. da Silva Leite, The systems containing clays and clay minerals from modified drug release: a review, Colloids Surf. B Biointerfaces 103 (2013) 642–651, https://doi.org/10.1016/j.colsurfb.2012.10.068.
[47] C. Aguzzi, P. Cerezo, C. Viseras, C. Caramella, Use of clays as drug delivery systems: possibilities and limitations, Appl. Clay Sci. 36 (2007) 22–36, https://doi.org/10.1016/j.clay.2006.06.015.
[48] J.K. Park, Y.Bin Choy, J.M. Oh, J.Y. Kim, S.J. Hwang, J.H. Choy, Controlled release of donepezil intercalated in smectite clays, Int. J. Pharm. 359 (2008) 198–204, https://doi.org/10.1016/j.ijpharm.2008.04.012.